Studies on the surface properties and fabrication method of mixed-matrix membrane for textile industry wastewater treatment

Teow Yeit Haan[a,b,*], Woo Sing Yee[b], Abdul Wahab Mohammad[a,b]

[a]*Research Centre for Sustainable Process Technology (CESPRO), Faculty of Engineering and Built Environment,*
Universiti Kebangsaan Malaysia, 43600 Bangi, Selangor, Malaysia, Tel. +603-89217095, email: yh_teow@ukm.edu.my (Y.H. Teow),
awm.ukm@gmail.com (A.W. Mohammad)
[b]*Chemical Engineering Programme, Faculty of Engineering and Built Environment, Universiti Kebangsaan Malaysia, 43600 Bangi,*
Selangor, Malaysia, email: wsy94030@hotmail.com (W.S. Yee)

ABSTRACT

In this study, the effect of embedding-titanium dioxide (TiO_2) nano particles(NPs) into the membrane matrix was studied using PVDF polymer and hydroxyl-functionalized PVDF (PVDF-OH) polymer as the polymer matrix for MMM synthesis via doping method and in-situ particle embedment method. The TiO_2 NPs size and its distribution into the membrane matrix were affected by the surface properties and the fabrication method of MMM. The improve TiO_2 NPs distribution through in-situ particle embedment method and with the use of PVDF-OH polymer was due to the weak hydrophobic/hydrophilic interactions between TiO_2 NPs and polymer solution. The permeate flux of MMMs was greatly enhanced with slight pore enlargement as well as the increasing of membrane hydrophilicity. However, the membrane pore enlargement does not scarify the MB rejection capability of MMMs as the presence of TiO_2 NPs created a strong electrostatic repulsion between MB ions and the surface of TiO_2 NPs, thus promising a great fouling mitigation effect. PVDF-OH/TiO_2 MMM fabricated through in-situ particle embedment method demonstrated the greatest permeate flux (20.22 ± 1.81 L/m² h) and MB rejection (99.45 ± 0.10%) with better antifouling properties due to larger effective surface area of TiO_2 NPs in membrane matrix.

Keywords: Mixed-matrix membrane; Surface properties; Fabrication method; Wastewater treatment; Membrane fouling

1. Introduction

The existence of dyes in water body has raised great attention due to their toxicology, carcinogenicity, and aesthetic effects [1]. The presence of dyes in water body will displease aesthetically and affect the nature of water, prevent light penetration, and subsequently reduce the photosynthetic activity in water [2]. Textile industry is one of the main contributors discharging the dyes into the environment. Methylene blue (MB) is extensively used in textile finishing [3].Numerous technologies have been applied for dyes removal from industrial effluent including adsorption [4,5], biodegradation [6,7], flocculation [8], and coagulation [9,10]. However, due to its non-biodegradability, biodegradation is inefficient to remove dyes from wastewater [11]. The sludge generation and disposal are the major draw backs raised from flocculation and coagulation processes [12]. Whereas, activated carbon, the most commonly used adsorbent in adsorption process is costly in terms of manufacturing and regeneration [13].

Based on several advantages including superior and constant quality of treated water, simple control or operation, energy saving, and environmentally-friendly outcomes, membrane technology has adopted for textile

*Corresponding author.

industry wastewater treatment [14–16]. However, hydrophobic nature is the most critical limitation of membrane in its dignified application as a valuable means of dyes removal as they exhibited susceptibility towards inherent problem of membrane fouling. Recent advances in combining nano technology and membrane technology has greatly expanded the avenues of membrane modification by introducing nano particles (NPs) into the membrane matrix for the fabrication of mixed-matrix membrane (MMM) to functionalize the membrane and concurrently enhancing its hydrophilicity, permeability, and fouling-resistance [17–19]. Good chemical stability, antibacterial property, and unique large surface-to-volume ratio of titanium dioxide (TiO_2) NPs make it an outstanding hydrophilic filler to be incorporated into membrane matrix [20,21].

Among the methods used to deposit the NPs into membrane material, the addition of NPs during dope preparation is considered as one of the most convenient methods to create the impact [22,23]. However, high surface energy of NPs often results in agglomeration due to poor mixing or shearing of the polymer solution as well as low stability of the colloid; leading to low functional surface area and defective of membrane pore morphology along with high surface roughness, which is a conspicuous drawback for applications. To increase homogeneous dispersity, reduce agglomeration, and improve stability of TiO_2 NPs, our previous studies were carried out to develop novel in-situ particle embedment method for MMM fabrication where the pore forming and TiO_2 embedding processes could be carried out during coagulation precipitation simultaneously [24,25].

Extended from the development of in-situ particle embedment method for membrane fabrication [24,25], effort was devoted to further enhance the TiO_2 NPs dispersion in membrane matrix by overcoming the high surface tension between TiO_2 NPs and the polymer matrix via hydroxylizing the polyvinylidene fluoride (PVDF) polymer through Fenton reaction [26]. It was shown that, the hydroxyl-functionalized PVDF (PVDF-OH) matrix could minimize the high surface tension between the hydrophilic TiO_2 NPs and hydrophobic polymer matrix, therefore promotes well distribution of TiO_2 NPs in MMM matrix. Although both doping method and in-situ particle embedment innovation in MMM production have been developed to incorporate TiO_2 NPs into the membrane polymer matrix; and PVDF-OH polymer was employed to further enhance the TiO_2 NPs dispersion in membrane matrix, to the best of our knowledge, no research work has been conducted in studying the effect surface properties and fabrication method of MMM towards its performance. It is an urgent need that this aspect should be explored to significantly contribute towards the feasible application of MMM. The aim of this work is to study the surface properties and fabrication method of mixed-matrix membrane for textile industry wastewater treatment.

2. Materials and methods

2.1. Materials

PVDF (Solvay, Shanghai) and N-N-dimethylacetamide (DMAc) (Merck, Germany) were used to fabricate the polymeric membrane. TiO_2 nano powder purchased from Aldach, Poland was used as the hydrophilic filler incorporated into the membrane matrix. Fenton's reagents used to functionalize the PVDF polymer consisted of ethanol (C_2H_5OH) (HmbG® Chemicals, Germany), iron (II) sulphate heptahydrate ($FeSO_4 \cdot 7H_2O$) (R & M Chemicals, UK), hydrogen peroxide (H_2O_2) (Bendosen, Norway), and sulphuric acid (H_2SO_4) (Avantor Performance Materials, USA). Methylene Blue (MB) (Merck, Germany) was used to prepare the feed solution for membrane performance study. Sodium dodecyl sulphate (SDS) (Aldrich Chemical Company Inc., USA) was dissolved in MB model solution as binding agent under vigorous stirring.

2.2. Synthesis of hydroxyl-functionalized PVDF (PVDF-OH) polymer

PVDF-OH polymer was synthesized via Fenton's reaction in which 18 g PVDF, 2.502 g $FeSO_4 \cdot 7H_2O$, 0.738 g H_2O_2, 90 mL C_2H_5OH, and 90 mL distilled water were reacted in a flask controlled at 50ºC using water bath for 1 h [26]. The resulted PVDF-OH polymer was filtered and washed with excess H_2SO_4 and water to remove the Fe^{3+} salt adsorbed onto the polymer. PVDF-OH polymer was then dried overnight in an oven at 70°C. The mechanism of hydroxylation was shown in equations below:

$$Fe^{2+} + H_2O_2 \rightarrow Fe^{3+} + HO^{\cdot} + OH^- \tag{1}$$

$$Fe^{3+} + H_2O_2 \rightarrow Fe^{2+} + HOO^{\cdot} + H^+ \tag{2}$$

The resulted hydroxyl group from Fenton's reaction will eventually bind to PVDF polymer as presented in Fig. 1.

2.3. Preparation of stable colloid suspension

TiO_2 colloidal suspension that used as coagulation water bath for membrane fabrication was prepared via chemical and mechanical methods. Chemical method was first carried out, followed by the mechanical method as described in our previous studies [24,26–28]. 0.01 g of TiO_2 nanopowder was added into 1 L of distilled water. pH of the TiO_2 colloidal suspension was adjusted by dropping HCl into the solution until it reached equilibrium at pH 4 to achieve electrostatic stability (zeta potential > ± 30 mV) with 200 nm of average hydrodynamic cluster size in suspension as reported in our previous studies [25,29]. The TiO_2 colloidal suspension was continued with mechanical method by subjecting to 15 min of ultrasonic irradiation to further break the agglomerated TiO_2 cluster. The colloidal stability was evaluated based on the zeta potential
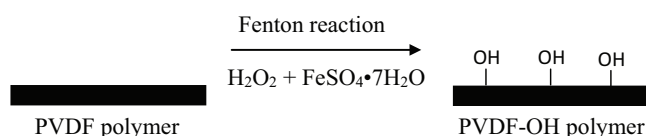
Fig. 1. Schematic diagram illustrating the process of PVDF polymer hydroxyl-functionalization.

and particle size distribution of TiO_2 NPs using Malvern Zetasizer ZS3600 (Malvern Instrument, UK) on the basis of DLS theory and cumulant method.

2.4. Membrane fabrication

2.4.1. Doping method

The membrane polymer solution was prepared by dissolving 18 g of PVDF polymer or PVDF-OH polymer in 82 g of DMAc. 0.01 g of TiO_2 nano powder was doped directly into the membrane polymer solution and the mixture was subjected to constant stirring of 250 rpm at 65°C for 4 h to form homogeneous solution. The homogeneous membrane polymer solution was then left overnight with stirring at 40°C and kept in a centrifuge tube [24,25]. PVDF/TiO_2 MMM and PVDF-OH/TiO_2 MMM were fabricated using a thin film applicator, Elcometer 4340 (Elcometer (Asia) Pte. Ltd., Singapore) on a flat glass plate at nominal thickness of 250 μm. The membrane casted on the glass plate was solidified by immediate immersing into coagulation water bath at room temperature (26°C) to avoid excessive surface evaporation [24,25].

2.4.2. In-situ particle embedment

In order to fabricate MMM through in-situ particle embedment method, TiO_2 NPs were introduced to the membrane matrix by immersing the casted membrane into the coagulation bath with TiO_2 colloidal suspension. The formulations of the fabricated membranes by both doping method and in-situ particle embedment method are summarized in Table 1.

2.5 Membrane characterization

2.5.1. Fourier transform infrared (FTIR) spectroscopy

FTIR spectra of PVDF and PVDF-OH polymer were obtained to investigate the functional groups on the polymer surface. The FTIR (Nicolet Nexus 670, USA) was equipped with an OMNI-sample attenuated total reflection (ATR) smart accessory and was coupled to a diamond crystal operated at incidence angle of 45°. Each spectrum, which was recorded at the average of 32 scans was taken with a resolution of 4 cm^{-1} and was collected at operating wave number ranging from 4000 – 425 cm^{-1}. The applied pressure was equal in all samples to avoid differences caused by the different penetrating depth.

2.5.2. Scanning electron microscope (SEM)

Top surface morphology and cross-sectional of the fabricated MMM were observed using SEM, Zeiss Evo MA 10 (Carl Zeiss Inc., Germany). For SEM observation, the membrane sample was cut into appropriate size and mounted on the sample holder. K 550 sputter coater was used to coat the outer surface of the membrane sample with a thin layer of gold under vacuum to provide electrical conductivity and to prevent the surface from being charged up. After gold sputtering, the membrane sample was examined under electron microscope at the potential of 10.0 kV.

2.5.3. Porosity and mean pore radius

Porosity (ε) and mean pore radius (r_m) of the fabricated membranes were determine by gravimetric method as defined by Eq. (3) and Guerout-Elford-Ferry equation as depicted by Eq. (4), respectively. Prior the porosity analysis, the membrane was soaked in distilled water for a day. Following, the water droplets on the membrane surface were wiped with filter paper and the weight of the wet membrane, W_w was weighed. Next, the membrane was dried in an oven at 60°C for a day and the weight of the dry membrane, W_d was weighed. Thickness of the membrane was measured using micro thickness gauge, Mitutoyo 7327 (Mitutoyo, Japan).

$$\varepsilon = \frac{(W_w - W_d)}{(\rho_w \times V)} \qquad (3)$$

where W_w and W_d are the weight of wet membrane (g) and dry membrane (g), respectively; ρ_w is the density of distilled water at room temperature (0.998 g/cm^3), and V is the volume of the membrane.

$$r_m = \sqrt{\left(\frac{(2.9 - 1.75\varepsilon) \times 8\eta l Q}{\varepsilon \times A \times \Delta P}\right)} \qquad (4)$$

where η is the viscosity of the water (Ns/m^2), l is the thickness of the membrane (m), Q is the volume of permeate per unit time (m^3/s), A is the effective surface area of the membrane (m^2), and ΔP is the operating pressure of the membrane (N/ m^2).

Table 1
Membrane nomenclatures and formulations for both doping method and in-situ particle embedment method

Membrane nomenclatures	PVDF/DMAc Ratio	PVDF-OH/DMAc Ratio	TiO_2 Concentration (g/L)	Fabrication Method
M1	18/82	–	–	–
M2	–	18/82	–	–
M3(a)	18/82	–	0.01	Doping
M3(b)	–	18/82	0.01	Doping
M4(a)	18/82	–	0.01	In-situ particle embedment
M4(b)	–	18/82	0.01	In-situ particle embedment

2.5.4. Atomic force microscope (AFM)

AFM, model NTEGRA PRIMA (NT-MDT America INC, Arizona) was employed to analyze the membrane surface roughness. The measurement was carried out at atmospheric pressure and the membrane was dried at room temperature prior analysis. Approximately 1 cm² of membrane sample was cut and affixed on top of the scanner tube. The membrane surface was then scanned with a laser beam reflected by the cantilever within a scanning area of 10 μm × 10 μm using the non-contact mode. Root mean square roughness (R_q) was recorded to indicate the membrane surface roughness.

2.5.5. Contact angle

The membrane wettability was characterized by contact angle of the membrane which was measured using contact angle meter, FM40Mk2 Easy Drop (Kruss GmbH, Germany) equipped with Drop Shape Analysis software. A droplet of deionized water (13 μL) was dropped onto the dry membrane surface using a microsyringe at room temperature (21 ± 1°C). Immediately, a microscope with long working distance 6.5× objective was used to capture the micro graphs at high frequency (100 Pcs/s).

2.5.6. Zeta potential

Membrane surface charge was measured using surface zeta potential cell, Malvern Zetasizer Nano ZS3600 (Malvern Instrument Inc., UK) with 300–350 nm latex particles as tracer particles. The dry membrane was first cut into small coupons and dipped into 0.1 mM NaCl at pH 7. It was then affixed at the measurement cell. The measurement cell was then inserted into the cell area to undertake the measurement.

2.6. Membrane performance study

2.6.1. Permeate flux and rejection

A laboratory bench-scale dead-end membrane filtration unit was used to study the performance of the fabricated membranes. The laboratory bench-scale dead-end membrane filtration unit mainly consists of a membrane dead-end filtration cell, Sterlitech HP 4750 (Sterlitech Corp., USA) with effective membrane surface area of 14.6 cm², nitrogen gas to exert pressure on membrane dead-end filtration cell, a stirrer to produce homogeneous model solution inside the membrane dead-end filtration cell throughout the membrane performance study, and a balance with data acquisition system to measure the weight of the permeate.

The membrane performance study was performed by laying the membrane on top of the membrane holder in membrane dead-end filtration cell and tightening with a rubber O-ring. Permeate flux of the membrane was determined using Eq. (5) by filtering the ultra-pure (UP) water at different transmembrane pressure of 1 bar, 3 bar, and 5 bar. Membrane permeability was obtained from the gradient of permeate flux against transmembrane pressure.

$$J = \frac{V}{At} \tag{5}$$

where J is the permeate flux (L/m²h), V is the permeate volume (L), A is the membrane effective surface area (m²), and t is the time taken to collect the permeate (h).

The effectiveness of the fabricated membranes was evaluated by using 20 mg/L MB solution as model solution. 300 mL of MB solution was added into the membrane dead-end filtration cell. The membrane rejection was evaluated at constant pressure of 3 bar and at stirring speed of 400 rpm to avoid concentration polarization. The concentration of model solution and permeate were determined by measuring its absorbance using UV-vis spectrophotometer at the wavelength of 662 nm. Membrane rejection towards MB solutes was calculated using Eq. (6).

$$R(\%) = \left(1 - \frac{C_p}{C_f}\right) \times 100\% \tag{6}$$

where R is the membrane rejection (%), C_p is the concentration of the permeate (mg/L), and C_f is the concentration of model solution (mg/L).

2.6.2. Fouling study

Membrane fouling study was performed continuously for 4 h using 20 mg/L MB solution as model solution. Fouling tendency of the membrane was assessed based on the normalized flux of the membrane throughout the membrane fouling study as expressed in Eq. (7).

$$\text{Normalized flux} = \frac{J_t}{J_p} \tag{7}$$

where J_t is the permeate flux at time t (L/m²h) and J_p is the initial permeate flux (L/m²h).

3. Results and discussion

3.1. Polymer characterization

The FTIR spectra of PVDF polymer and PVDF-OH polymer were presented in Fig. 2. It was interesting to notice that PVDF-OH polymer was possessed a broad
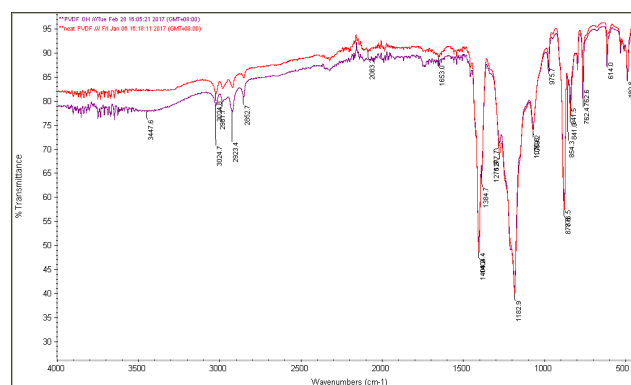
Fig. 2. FTIR spectra of PVDF polymer and PVDF-OH polymer.

band around 3500–3000 cm^{-1} in FTIR spectra compared to PVDF polymer, corresponded to the hydroxyl functional group which has been introduced to PVDF polymer [30,31]. The presence of hydroxyl functional group on PVDF-OH polymer could increase the hydrophilicity of PVDF-OH membrane, which consequently increased the membrane permeate flux.

3.2. Membrane characterization

3.2.1. SEM

Top surface and cross-sectional SEM micro graphs of the fabricated membranes prepared from different formulations are shown in Fig. 3. As depicted in Fig. 3a under 5.00 k× magnification, larger and uneven pore structure

(a)   (b)
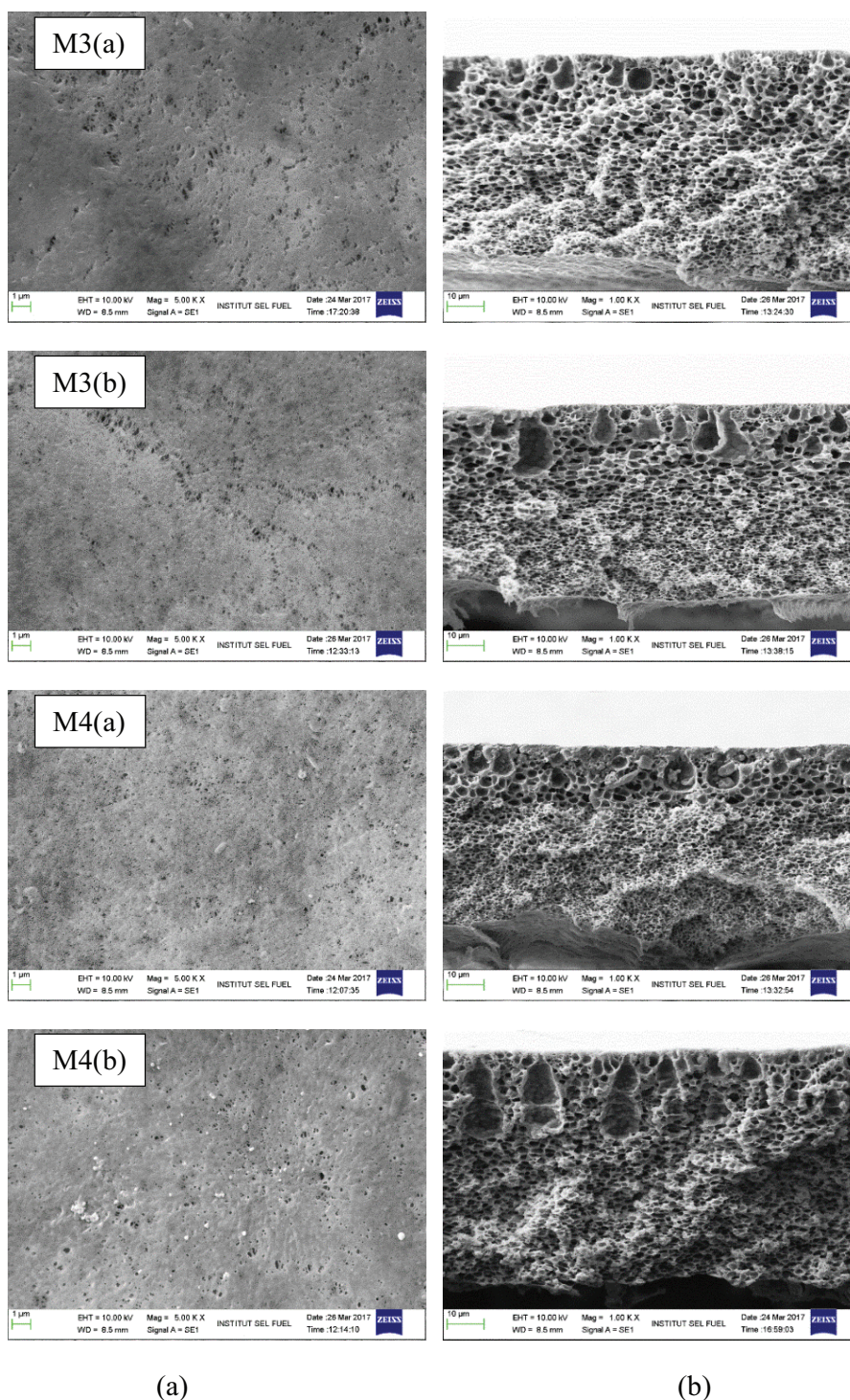
Fig. 3(a) Top surface and (b) cross-sectional SEM micro graphs of the membranes fabricated prepared from different formulations.

was appeared on the surface of MMMs fabricated from doping method (M3(a) and M3(b)) while for the MMMs fabricated from in-situ particle embedment method (M4(a) and M4(b)), smaller and cellular pore structure was observed. The experimental results indicated that membrane fabrication method was the dominant factor contributed to the structural change of membrane morphology.

Among the methods used to enhance the hydrophilicity of membrane, the addition of hydrophilic additive into membrane polymer solution through doping method is generally considered as one of the most convenient methods to create the impact [22,23]. However, introducing of high surface energy TiO_2 NPs through doping method caused the stretching effect during phase inversion process, which induced NPs to aggregate and resulted poor NPs distribution in the membrane matrix and/or defective pore structure of the membrane. On the other hand, MMMs incorporated with TiO_2 NPs through in-situ particle embedment method do not present any significance effect on membrane structure.

The morphological changes of membrane cross-sectional structure could be related to the rate of solvent-nonsolvent inter-diffusion during the phase inversion process. PVDF-OH polymer with the presence of hydroxyl functional group was having higher affinity to the water. This will promote higher solvent out flux and non-solvent influx [32,33]. Improved miscibility of membrane polymer solution with water momentously increased the polymer concentration at the interface due to higher solvent out flux. As a result, membrane with longer macro void was produced for MMMs fabricated from PVDF-OH polymer (as presented by M3(b) and M4(b)).

3.2.2. Porosity and mean pore radius

Porosity and mean pore radius of the fabricated membranes are tabulated in Table 2. Generally, there was no significant difference for the porosity of the fabricated membranes where the membrane porosity ranged from $41.3 \pm 1.11\%$ to $48.6 \pm 3.13\%$. However, the mean pore radius of the fabricated membranes was increased with the incorporation of TiO_2 NPs into membrane matrix. The mean pore radius enlargement was owing to the increase of stress/tension between polymer and TiO_2 NPs, resulted from the organic shrinkage that occurred during precipitation process of wet-casting polymeric membrane, whereby both hydrophobic polymer and hydrophilic TiO_2 NPs were tend to minimize their surface by shrinking. Consequently, membrane with bigger pores was formed [25].

In addition, the use of PVDF-OH polymer for membrane fabrication had also contributed to the slight increase of membrane mean pore radius. PVDF-OH polymer would increase the exchange rate between solvent and non-solvent during phase inversion process which consequently enhanced the instantaneous liquid-liquid demixing. The spinodal demixing process was likely devoted to an increase in membrane mean pore radius [34].

Whereas, pore size narrowing was noticed for MMMs fabricated from doping method compared to the MMMs fabricated from in-situ embedment method. Pore narrowing effect was due to pore blocking of MMMs attributed to poor stability of TiO_2 NPs in membrane polymer solution,

Table 2
Porosity and mean pore radius of the fabricated membranes

Membranes	Porosity (%)	Mean pore radius (μm)
M1	44.0 ± 1.82	5.65 ± 0.16
M2	45.7 ± 1.14	6.21 ± 0.13
M3(a)	45.7 ± 1.47	6.56 ± 0.11
M3(b)	41.3 ± 1.11	8.08 ± 0.14
M4(a)	48.6 ± 3.13	7.91 ± 0.32
M4(b)	44.9 ± 1.27	9.22 ± 0.20

which was the main drawback of doping method in membrane modification. High surface tension between TiO_2 NPs and the membrane matrix resulted in defective membrane pore structure might reduce the intrinsic membrane permeability [35].

3.2.3. AFM

Fig. 4 shows the AFM three-dimensional micro graphs of membrane surfaces fabricated with different formulations. In these micro graphs, the brightest area represents the highest point on the membrane surface, whereas the dark region indicates the valleys or membrane pores. In general, all membrane surfaces presented in Fig. 4 were not smooth. The surface roughness parameter of the membrane was expressed in terms of root mean square value of Z data (R_q), which is tabulated in Table 3.

Table 3 shows that the surface roughness of the fabricated membranes was greatly changed by the fabrication method and the properties of the polymer used. Generally, R_q value of PVDF-OH membranes was apparently lower than that of PVDF membranes. At equal TiO_2 concentration and with the same fabrication method, better dispersion of TiO_2 NPs within PVDF-OH polymer matrix reduced the surface roughness of PVDF-OH membranes due to lower surface energy between PVDF-OH polymer and TiO_2 NPs. Smoother surface of PVDF-OH membranes with less degree of clustering and agglomeration was expected to have low fouling tendency [36,37]. On the other hand, the surface morphology was greatly changed by the clustering effect of TiO_2 NPs assembled on membrane through doping method in membrane fabrication. Whereas, membrane fabrication through in-situ particle embedment method could reduce the occurrence of TiO_2 NPs agglomeration and subsequently improved the surface roughness of the membranes. It was postulated that the advantages of hydrophilic TiO_2 NPs embedment could be realized when the particles were uniformly distributed within the polymeric matrix.

3.2.4. Contact angle

Membrane surface wettability in this study was determined using contact angle measurement. The static deionized water contact angles of the fabricated membranes are shown in Fig. 5. In general, lower the contact angle, the more hydrophilic membrane will be.
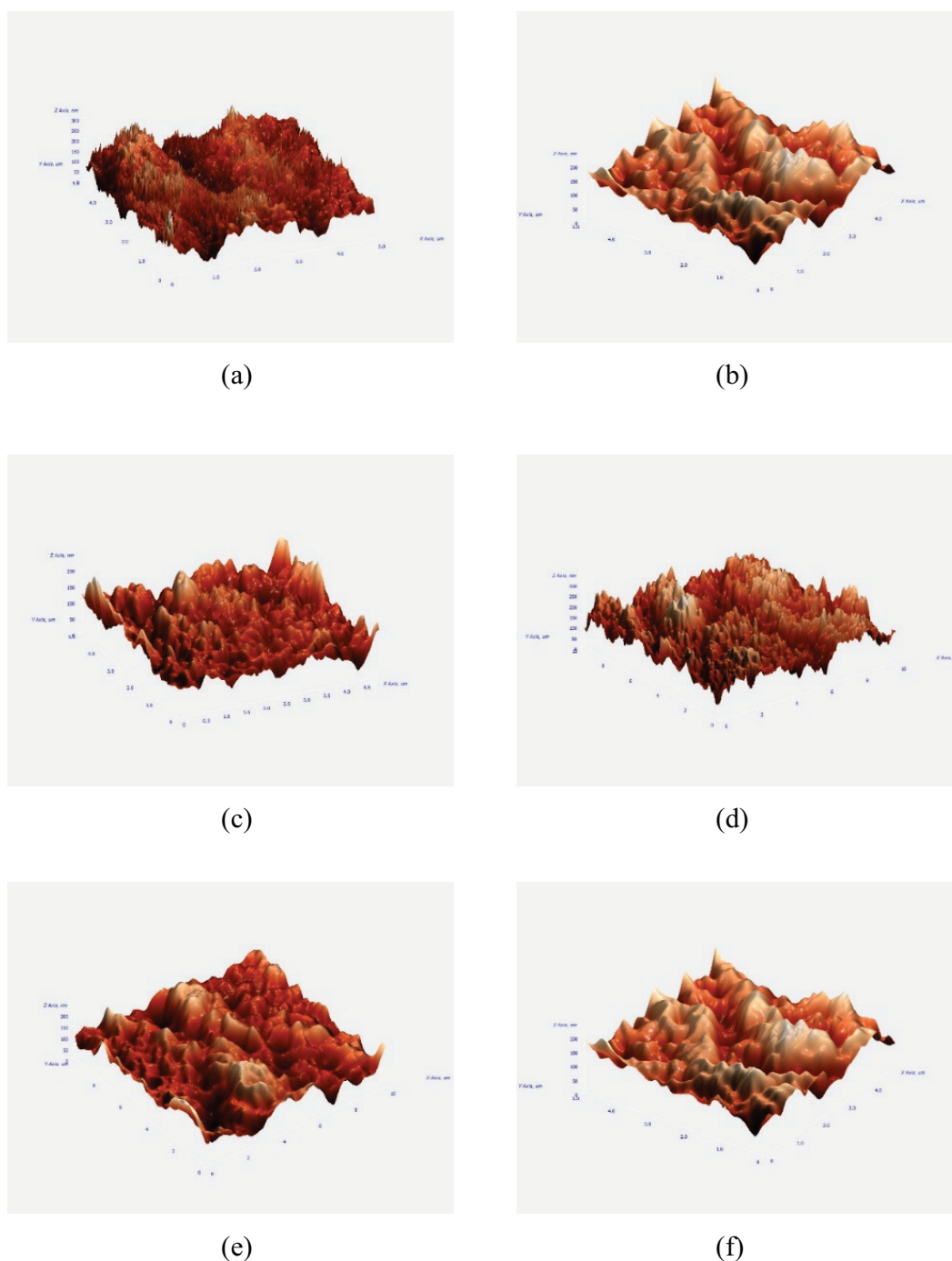
Fig. 4. AFM three-dimensional micro graphs of membrane surface (a) M1 (b) M2 (c) M3(a) (d) M3(b) (e) M4(a) and (f) M4(b).

Membrane surface wettability is governed by chemical composition as well as geometric structure of the membrane surface [25]. It was found that the contact angles of neat membranes were lower than that of MMMs. Theoretically, MMMs were expected to exhibit lower contact angle value due to the incorporation of hydrophilic TiO_2 NPs into the membrane matrix and lower surface roughness parameter. However, contact angle was not only affected by hydrophilicity and surface roughness. It was also contributed by surface pore size, porosity, and pore size distribution. Higher porosity and larger mean pore radius of MMMs create more air gaps between the polymer and water, where deionized water droplet was not able to directly in contact with the membrane surface, thus impaired the membrane surface wettability.

On the other hand, the contact angles of MMMs fabricated from doping method were slightly higher than that of MMMs fabricated through in-situ particle embedment. This

Table 3
Root mean square value for the membrane surface

Membranes	R_q (nm)
M1	39.436
M2	37.869
M3(a)	32.815
M3(b)	35.196
M4(a)	33.330
M4(b)	30.365

Note: The root mean square value of Z data (R_q) is the standard deviation of the Z values within the given area.
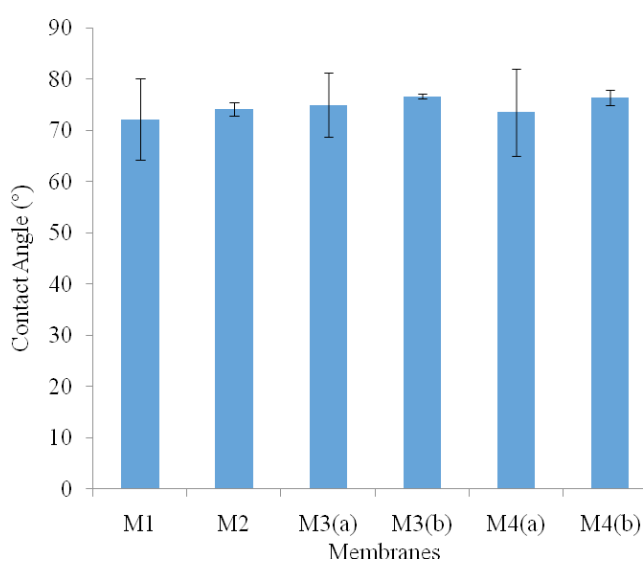
Fig. 5. Static deionized water contact angle of the fabricated membranes with different formulations.

was attributed to the higher surface roughness of MMMs fabricated from doping method. This postulation was in good agreement with Rana and Matsuura [38] report who found that the contact angle values of membranes with higher surface roughness were higher compared to membranes with lower surface roughness, even if both membranes have the similar hydrophilicity.

Additionally, the contact angle was increased for the MMMs fabricated from PVDF-OH polymer compared to MMMs fabricated from PVDF polymer despite the membrane fabrication method. This finding was unexpected as MMMs fabricated from PVDF-OH polymer were exhibited lower surface roughness parameter and porosity compared to MMMs fabricated from PVDF polymer. The further increase of contact angle for MMMs fabricated from PVDF-OH polymer was probably due to larger mean pore radius created which was the predominant factor that compensate the membrane surface wettability where deionized droplet could not directly in contact with flat horizontal surface of PVDF-OH MMMs.

Membrane hydrophilicity/hydrophobicity is a complicated phenomenon. Although deposition of TiO_2 NPs into the membrane matrix, doping method, and the used

of PVDF-OH polymer showed an increasing trend in contact angle for the membranes, it does not mean that these approaches have reduced the membrane hydrophilicity. Ngang et al. [35] and Teow et al. [25] had reported that MMMs incorporated with TiO_2 NPs were exhibiting higher permeate flux despite the increment in contact angle.

3.2.5. Zeta potential

In addition to hydrophilic character, membrane which possesses more negative charge on the top selective layer will also contribute in lowering the membrane fouling propensity. The zeta potential of the fabricated membranes at pH 7 is revealed in Fig. 6.

Although all membranes were negatively charged when dipping into 0.1 mM NaCl solution at pH 7 environment, the incorporation of TiO_2 NPs into membrane matrix makes the surface more negative. The negative charge of the neat membranes was due to the presence of dipolar polarization (orientation polarization) effect inherent by PVDF polar molecules on the base polymer and thus the preferential adsorption of negative chloride ions from the solution [39]. On the other hand, the increasing net negative charge on MMMs compared to neat membranes was attributed to the presence of TiO_2 NPs. The isolectric point (IEP) of TiO_2 NPs was reported to be ~pH 6.3 [40], so for MMMs dipping into NaCl solution at pH 7, where the pH was greater than the IEP of TiO_2 NPs, the membranes would be more negatively charged.

Different membrane fabrication method possesses different extent of increment in membrane surface charge for MMMs incorporated with the same TiO_2 concentration. Fig. 6 depicts that MMMs fabricated through in-situ particle embedment presented slightly higher zeta potential value compared to MMMs fabricated from doping method. This could be due to fairly well TiO_2 NPs distribution on MMMs-surface fabricated through in-situ particle embedment. The lesser degree of TiO_2 NPs clustering in MMMs prepared using in-situ particle embedment increased the effective surface area of TiO_2 NPs which consequently increased the negative charge of the membrane.

3.3. Membrane performance study

3.3.1. Permeate flux and rejection

Table 4 summarizes the performance of the fabricated membranes in terms of permeate flux and MB rejection. Both reported permeate flux and MB rejection values were corresponded to the average of three replications with the membrane tested was randomly chosen among the independent sheets.

Comparing the permeate flux for all membranes, MMMs permeate flux was improved by embedding TiO_2 NPs into the membrane matrix, even though there was an increment in terms of contact angle for MMMs, confirming the effect of TiO_2 NPs on membrane permeate flux enhancement. This result was coincides with the findings of Luo et al. [41] who demonstrated that the permeate flux and retention of TiO_2 composite membrane were increased greatly from 70.2 L/ m^2 h to 102.9 L/ m^2 h and from 21.9% to 34.5%, respectively as compared to neat UF polyether sulfone
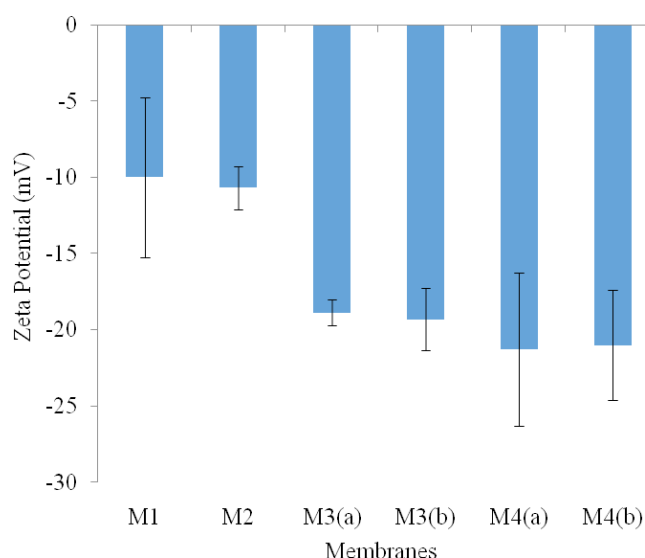
Fig. 6. Zeta potential of the fabricated membranes with different formulations.

Table 4
Permeate flux and MB rejection of the fabricated membranes with different formulations

Membranes	Permeate flux (L/m² h)	Rejection (%)
M1	9.66 ± 1.47	98.75 ± 0.14
M2	12.41 ± 2.81	98.94 ± 0.28
M3(a)	13.03 ± 0.57	99.41 ± 0.07
M3(b)	16.43 ± 3.47	99.46 ± 0.05
M4(a)	19.89 ± 0.89	99.47 ± 0.05
M4(b)	20.22 ± 1.81	99.45 ± 0.10

membrane for polyethylene glycol-5000 separation. The enhanced permeate flux of MMMs upon integration of TiO_2 NPs was due to higher affinity of TiO_2 NPs towards water [42]. Hydroxyl group on TiO_2 NPs surface will attract more water molecules to pass through the membrane pores [43].

On the other hand, PVDF-OH membranes were apparently gave higher permeate flux than that of PVDF membranes. Hydroxyl functional group credited by PVDF-OH polymer in PVDF-OH membranes caused partial hydrolysis on the membrane surface and help to reduce the hydrophobic adsorption between the MB ions and membrane surface, thus enhanced the membrane permeate flux. It was also proposed that the better TiO_2 NPs dispersion in PVDF-OH MMMs and through in-situ particle embedment method offered larger effective surface area for NPs, which increased the number of adsorption sites for water molecules on the membrane surface as reported in our previous study [26]. Water molecules were attracted into PVDF-OH MMMs matrix and promoted to penetrate through. Where as, high aggregation tendency of TiO_2 NPs in MMMs fabricated through doping method might block the membrane pores during immersion precipitation and reduced the membrane permeate flux. Another plausible reason for the permeate flux enhancement as shown by MMMs fabri-

cated using PVDF-OH polymer and through in-situ particle embedment method was denoted to the increasing of mean pore radius attributed to the nano gap between TiO_2 NPs and the polymer matrix as reported in Table 2 [25].

Besides the permeate flux, removal efficiency of MB was found to be affected by the presence of TiO_2 NPs in the membrane matrix. Table 4 demonstrated that MMMs have increased the membrane permeate flux without scarifying the MB rejection capability, suggesting the incorporation of hydrophilic TiO_2 NPs had promised a great fouling mitigation effect. The increasing negative charge on MMMs surface attributed to the presence of TiO_2 NPs created a strong electrostatic repulsion between MB ions and the surface of TiO_2 NPs. Therefore, in addition to hydrophilic character, MMMs with the incorporation of TiO_2 NPs have provided additional advantage in enhancing the membrane rejection.

3.3.2. Fouling study

The flux data resulted from successive filtration are illustrated in Fig. 7 in terms of normalized flux ratio (J/J_O), which is the instantaneous flux over the initial flux. The membrane fouling tendency was clearly revealed by normalized flux reduction of 53.7%, 48.89%, 46.75%, 41.11%, 46.39%, and 38.61% for M1, M2, M3(a), M3(b), M4(a), and M4(b), respectively after 4 h of MB filtration.

Generally, MMMs were found to have more fouling resistance compared to neat membranes. Different fouling behaviour could be attributed to the different surface properties of the membranes. MMMs with the incorporation of hydrophilic TiO_2 NPs into the membrane matrix had reduced the fouling propensity of the membrane due to higher affinity of TiO_2 to water. As reported in the literature, the anti-fouling activity of MMMs was attributed to the water shielding effect of the hydrophilic –OH group on TiO_2 NPs surface [44,45]. Despite the membrane hydrophilicity that has been improved by incorporating TiO_2 NPs, lower surface roughness parameter of MMMs also led to poorer fouling properties compared to the neat membranes. Cao et al. [36] found that the membrane roughness was the most influential factor on membrane anti-fouling capability under the same operating conditions. Coarser neat membranes were much easy to absorb MB ions from water compared to smoother MMMs surface with lower surface roughness and surface energy. Subsequent accumulation of MB ions on neat membrane surface resulted in a diminishing of effective membrane pore size [46], leading to further physical retention, and causing an increase in hydraulic resistance[47].

On the other hand, the membrane fouling propensity was greatly reduced in PVDF-OH MMM system where the membranes were fabricated from PVDF-OH polymer. The improvement of the membranes' anti-fouling potential was primarily resulted from smoother surface layer and higher membrane surface charge attributed by the enhancement of TiO_2 NPs distribution in membrane matrix where the hydrophobic adsorption between MB ions and the membrane surface was momentously diminished. Whereas, TiO_2 clustering effect resulted from MMMs fabricated through doping method provides extra hydraulic resistance had slightly compensating the hydrophilic nature of TiO_2 NPs
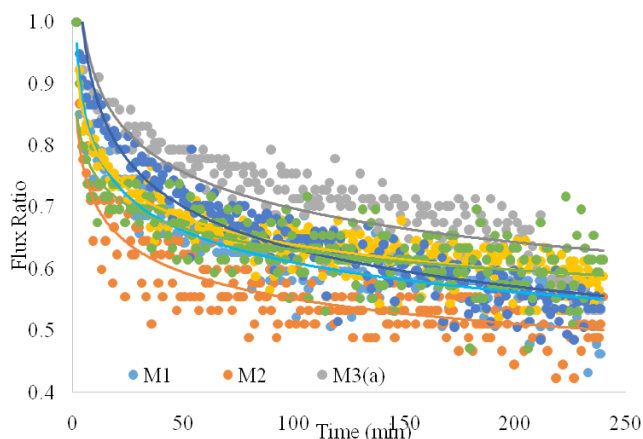
Fig. 7. Experimental dead-end MB filtration data for all fabricated membranes with different formulations.

deposited on MMMs. It was suggested that the advantages of NPs embedment can only be realized when the particles were uniformly distributed within the polymeric matrix.

4. Conclusion

As a summary, the effect of embedding TiO_2 NPs into the membrane matrix using PVDF polymer and PVDF-OH polymer via Fenton reaction as the polymer matrix for MMM synthesis via doping method and in-situ particle embedment method was developed in this study. Surface properties and fabrication method had greatly affected the formation of MMM. Membranes fabricated using PVDF-OH polymer and through in-situ particle embedment method was found to have better TiO_2 NPs particle distribution compared to the membranes fabricated using PVDF polymer and through doping method. The enhancement of TiO_2 NPs particle distribution was contributed by lower surface energy between PVDF-OH polymer and TiO_2 NPs; and in-situ particle embedment method which could minimize the surface tension between hydrophilic TiO_2 NPs and hydrophobic polymer matrix.

Generally, the permeate flux of MMMs was improved as compared to the neat membrane. It was mainly due to slight pore enlargement, higher membrane porosity as well as the increasing of membrane hydrophilicity with the embedment of TiO_2 NPs into the membrane matrix. However, the membrane pore enlargement does not scarify the MB rejection capability of MMMs attributed to the presence of TiO_2 NPs created a strong electrostatic repulsion between MB ions and the surface of TiO_2 NPs deposited on the membrane surface, thus promising a great fouling mitigation effect. Smoother surface of PVDF-OH MMM fabricated through in-situ particle embedment with less degree of clustering and higher membrane surface charge was demonstrated the greatest permeate flux (20.22 ± 1.81 L/m² h) and MB rejection (99.45 ± 0.10%) with better anti fouling properties due to larger effective surface area of TiO_2 NPs in membrane matrix. By having better anti fouling property, the frequency of membrane cleaning and membrane replacement can be greatly reduced. This would eventually save the operation cost of membrane filtration process and can be contribute as an effort to solve the drawback of membrane technology.

References

[1] S. Chen, J. Zhang, C. Zhang, Q. Yue, Y. Li, C. Li, Equilibrium and kinetic studies of methyl orange and methyl violet adsorption on activated carbon derived from Phragmites australis, Desalination, 252 (2010) 149–156.

[2] J. Babu, Z.V.P. Murthy, Treatment of textile dyes containing waste waters with PES/PVA thin film composite nano filtration membranes, Sep. Purf. Tech., 183 (2017) 66–72.

[3] J. He, A. Cui, S. Deng, J.P. Chen, Treatment of methylene blue containing wastewater by a cost-effective micro-scale biochar/polysulfone mixed matrix hollow fiber membrane: Performance and mechanism studies, J. Colloid Interf. Sci., 512 (2018) 190–197.

[4] H.-F. Qian, G. Feng, G. Bai, Y.-C. Liu, L.-L. Hu, A contrastive study of adsorption behaviors on polyurethane fiber with diester/diurethane tethered and non-tethered azo disperse dyes, Dyes Pigm., 145 (2017) 301–306.

[5] F. Jiang, D.M. Dinh, Y.-L. Hsieh, Adsorption and desorption of cationic malachite green dye on cellulose nano fibril aerogels, Carbohyd. Polym., 173 (2017) 286–294.

[6] S. Ortiz-Monsalve, J. Dornelles, E. Poll, M. Ramirez-Castrillón, P. Valente, M. Gutterres, Biodecolourisation and biodegradation of leather dyes by a native isolate of Trametes villosa, Process Saf. Environ., 109 (2017) 437–451.

[7] W. Sun, C. Zhang, J. Chen, B. Zhang, H. Zhang, Y. Zhang, L. Chen, Accelerating biodegradation of a mono azo dye Acid Orange 7 by using its endogenous electron donors, J. Hazard. Mater., 324 (2017) 739–743.

[8] E. GilPavas, I. Dobrosz-Gómez, M.Á. Gómez-García, Coagulation-flocculation sequential with Fenton or Photo-Fenton processes as an alternative for the industrial textile wastewater treatment, J. Environ. Manage., 191 (2017) 189–197.

[9] W. Wang, Q. Yue, R. Li, W. Song, B. Gao, X. Shen, Investigating coagulation behavior of chitosan with different Al species dual-coagulants in dye wastewater treatment, J. Taiwan Inst. Chem. E., 78 (2017) 423–430.

[10] R. Li, B. Gao, K. Guo, Q. Yue, H. Zheng, Y. Wang, Effects of paper making sludge-based polymer on coagulation behavior in the disperse and reactive dyes wastewater treatment, Bioresource Technol., 240 (2017) 59–67.

[11] S. Seshadri, P.L. Bishop, A.M. Agha, Anaerobic/aerobic treatment of selected azo dyes in wastewater, Waste Manage., 14 (1994) 127–137.

[12] M. Unlu, H. Yukseler, U. Yetis, Indigo dyeing wastewater reclamation by membrane-based filtration and coagulation processes, Desalination, 240 (2009) 178–185.

[13] S. Wang, Z.H. Zhu, A. Coomes, F. Haghseresht, G.Q. Lu, The physical and surface chemical characteristics of activated carbons and the adsorption of methylene blue from wastewater, J. Colloid Interf. Sci., 284 (2005) 440–446.

[14] M. Dilaver, S.M. Hocaoğlu, G. Soydemir, M. Dursun, B. Keskinler, İ. Koyuncu, M. Ağtaş, Hot wastewater recovery by using ceramic membrane ultra filtration and its re-usability in textile industry, J. Clean. Prod., 171 (2018) 220–233.

[15] E. Hassanzadeh, M. Farhadian, A. Razmjou, N. Askari, An efficient wastewater treatment approach for a real woolen textile industry using a chemical assisted NF membrane process, Environ. Nanotechnol. Monitor. Manage., 8 (2017) 92–96.

[16] T.V. Luong, S. Schmidt, S.A. Deowan, J. Hoinkis, A. Figoli, F. Galiano, Membrane Bioreactor and promising application for textile industry in Vietnam, Procedia CIRP, 40 (2016) 419–424.

[17] P.V. Chai, E. Mahmoudi, Y.H. Teow, A.W. Mohammad, Preparation of novel polysulfone-Fe$_3$O$_4$/GO mixed-matrix membrane for humic acid rejection, J. Water Process Eng., 15 (2017) 83–88.

[18] K.C. Ho, Y.H. Teow, W.L. Ang, A.W. Mohammad, Novel GO/OMWCNTs mixed-matrix membrane with enhanced antifouling property for palm oil mill effluent treatment, Sep. Purf. Tech., 177 (2017) 337–349.

[19] Y. Liu, F. Li, Q. Xia, J. Wu, J. Liu, M. Huang, J. Xie, Conductive 3D sponges for affordable and highly-efficient water purification, Nano scale (2018).

[20] N.A.A. Hamid, A.F. Ismail, T. Matsuura, A.W. Zularisam, W.J. Lau, E. Yuliwati, M.S. Abdullah, Morphological and separation performance study of polysulfone/titanium dioxide (PSF/TiO$_2$) ultra filtration membranes for humic acid removal, Desalination, 273 (2011) 85–92.

[21] F. Li, F. Zhao, M. Huang, C. Ma, B. Yang, Q. Tian, Thin-film composite membranes with nano composite substrate modified with graphene oxide/TiO$_2$ for forward osmosis process, Desal. Water Treat., 70 (2017) 64–78.

[22] M. Peyravi, A. Rahimpour, M. Jahanshahi, A. Javadi, A. Shockravi, Tailoring the surface properties of PES ultra filtration membranes to reduce the fouling resistance using synthesized hydrophilic copolymer, Micropor. Mesopor. Mater., 160 (2012) 114–125.

[23] L. Zhao, W.S.W. Ho, Novel reverse osmosis membranes incorporated with a hydrophilic additive for seawater desalination, J. Membrane Sci., 455 (2014) 44–54.

[24] Y.H. Teow, A.L. Ahmad, J.K. Lim, B.S. Ooi, Preparation and characterization of PVDF/TiO$_2$ mixed matrix membrane via in situ colloidal precipitation method, Desalination, 295 (2012) 61–69.

[25] Y.H. Teow, PVDF-TiO$_2$ mixed-matrix membrane with anti-fouling properties for humic acid removal, Malaysia, Universiti Sains Malaysia, 2014.

[26] Y.H. Teow, A.A. Latif, J.K. Lim, H.P. Ngang, L.Y. Susan, B.S. Ooi, Hydroxyl functionalized PVDF–TiO$_2$ ultra filtration membrane and its anti fouling properties, J. Appl. Polym. Sci., 132(21) (2015) 1–11.

[27] Y.H. Teow, A.L. Ahmad, J.K. Lim, B.S. Ooi, Studies on the surface properties of mixed-matrix membrane and its anti fouling properties for humic acid removal, J. Appl. Polym. Sci., 128 (2013) 3184–3192.

[28] Y.H. Teow, B.S. Ooi, A.L. Ahmad, Fouling behaviours of PVDF-TiO$_2$ mixed-matrix membrane applied to humic acid treatment, J. Water Process Eng., 15 (2017) 89–98.

[29] Y.H. Teow, A.L. Ahmad, B.S. Ooi, Surface chemistry and dispersion property of titanium dioxide nano particles in water suspension, Global J. Environ. Sci. Tech., 2 (2012) 1–6.

[30] A. Teleki, M.K. Akhtar, S.E. Pratsinis, The quality of SiO$_2$-coatings on flame-made TiO$_2$-based nano particles, J. Mater. Chem., 18 (2008) 3547–3555.

[31] S.I. Seok, J.H. Kim, TiO$_2$ nano particles formed in silica sol–gel matrix, Mater. Chem. Phys., 86 (2004) 176–179.

[32] P. Vandezande, X. Li, L.E.M. Gevers, I.F.J. Vankelecom, High throughput study of phase inversion parameters for polyimide-based SRNF membranes, J. Membr. Sci., 330 (2009) 307–318.

[33] J. Lee, H.-R. Chae, Y.J. Won, K. Lee, C.-H. Lee, H.H. Lee, I.-C. Kim, J.-m. Lee, Graphene oxide nano platelets composite membrane with hydrophilic and anti fouling properties for wastewater treatment, J. Membr. Sci., 448 (2013) 223–230.

[34] P. van de Witte, P.J. Dijkstra, J.W.A. van den Berg, J. Feijen, Phase separation processes in polymer solutions in relation to membrane formation, J. Membr. Sci., 117 (1996) 1–31.

[35] H.P. Ngang, A.L. Ahmad, S.C. Low, B.S. Ooi, Preparation of mixed-matrix membranes for micellar enhanced ultra filtration based on response surface methodology, Desalination, 293 (2012) 7–20.

[36] X. Cao, J. Ma, X. Shi, Z. Ren, Effect of TiO$_2$ nano particle size on the performance of PVDF membrane, Appl. Surf. Sci., 253 (2006) 2003–2010.

[37] A. Idris, N. Mat Zain, M.Y. Noordin, Synthesis, characterization and performance of asymmetric polyether sulfone (PES) ultra filtration membranes with polyethylene glycol of different molecular weights as additives, Desalination, 207 (2007) 324–339.

[38] D. Rana, T. Matsuura, Surface modifications for anti fouling membranes, Chem. Rev., 110 (2010) 2448–2471.

[39] D.B. Burns, A.L. Zydney, Buffer effects on the zeta potential of ultra filtration membranes, J. Membr. Sci., 172 (2000) 39–48.

[40] K.E. O'Shea, C. Cardona, The reactivity of phenol in irradiated aqueous suspensions of TiO$_2$. Mechanistic changes as a function of solution pH, J. Photo chem. Photo bio A., 91 (1995) 67–72.

[41] M.-L. Luo, J.-Q. Zhao, W. Tang, C.-S. Pu, Hydrophilic modification of poly (ether sulfone) ultra filtration membrane surface by self-assembly of TiO$_2$ nano particles, Appl. Surf. Sci., 249 (2005) 76–84.

[42] T.-H. Bae, T.-M. Tak, Preparation of TiO$_2$ self-assembled polymeric nano composite membranes and examination of their fouling mitigation effects in a membrane bioreactor system, J. Membr. Sci., 266 (2005) 1–5.

[43] M.M. Bello, M.M. Nourouzi, L.C. Abdullah, T.S.Y. Choong, Y.S. Koay, S. Keshani, POME is treated for removal of color from biologically treated POME in fixed bed column: Applying wavelet neural network (WNN), J. Hazard. Mater., 262 (2013) 106–113.

[44] S.S. Madaeni, N. Ghaemi, Characterization of self-cleaning RO membranes coated with TiO$_2$ particles under UV irradiation, J. Membr. Sci., 303 (2007) 221–233.

[45] S.S. Madaeni, N. Ghaemi, A. Alizadeh, M. Joshaghani, Influence of photo-induced super hydro philicity of titanium dioxide nano particles on the anti-fouling performance of ultra filtration membranes, Appl. Surf. Sci., 257 (2011) 6175–6180.

[46] H.K. Shon, S. Vigneswaran, H.H. Ngo, J.H. Kim, Chemical coupling of photo catalysis with flocculation and adsorption in the removal of organic matter, Water Res., 39 (2005) 2549–2558.

[47] J. Cho, G. Amy, J. Pellegrino, Membrane filtration of natural organic matter: initial comparison of rejection and flux decline characteristics with ultra filtration and nano filtration membranes, Water Res., 33 (1999) 2517–2526.